Laser Physics, Vol. 4, No. 5, 1994, pp. 1085 - 1092.

SPECIAL ISSUE
"LASER COOLING AND TRAPPING"

Effects of Hyperfine Structure on Alkali Trap-Loss Collisions

T. Walker* and D. Pritchard**

** Department of Physics, University of Wisconsin at Madison, Madison, WI 53706, USA*
*** Department of Physics and Research Laboratory of Electronics, Massachusetts Institute of Technology, Cambridge, MA 02139, USA*

Received July 29, 1993

Abstract – We present calculations of the hyperfine structure of alkali-dimer resonance potential curves in the regime where the resonant dipole–dipole interaction is comparable to the hyperfine interaction. We discuss the implications of these curves for the dynamics of excited-state collisions between optically trapped alkali atoms.

1. INTRODUCTION

Optical trapping and cooling techniques produce atomic vapors with microkelvin temperatures and densities of 10^{10} cm^{-3} or more. Under these conditions, inelastic (superelastic) collisions between the atoms can give the atoms sufficient kinetic energy to eject them from the trap. Since these "trap-loss" collisions limit the number of atoms that can be trapped, their effects can be easily (though indirectly) observed. Recent experiments [1 - 3] have shown the importance of hyperfine interactions on the dynamics of these collisions. In this paper, we present calculations of the adiabatic potential curves, including hyperfine structure, that are relevant to understanding these effects. We also make estimates of the adiabaticity of the motion and predict new features in the trap-loss spectra.

Trap-loss collisions of alkali atoms can be roughly grouped into those that involve both atoms being in the ground electronic state during the collision or those that involve excited electronic states. The excited-state collisions are of fundamental interest because of the importance of radiation fields in determining the collision dynamics. In particular, spontaneous emission can interrupt the collision process if the collision time is comparable to the spontaneous lifetime of the excited state. This implies that the conventional concept of an excited-state collision, where the collision partners are prepared in well-defined initial molecular states that evolve coherently during the collision, must be modified.

Current wisdom is that, at low temperatures, an excited-state collision is better thought of as beginning with excitation of an atom pair in the ground state by a photon from a laser, followed by acceleration of the atoms toward each other by the strongly attractive excited-state potential [$V(R) = -C_3R^{-3}$, where R is the interatomic separation]. If the acceleration is strong enough to bring the atoms close together before spontaneous emission occurs, an energy transfer process can occur that gives the atoms sufficiently large kinetic energy that they cannot be contained by the trap. On the other hand, if spontaneous emission occurs before the atoms reach the energy transfer region at small interatomic distances, the collision continues on the much weaker ground-state potential curve, and at the conclusion of the collision, the atoms are still cooled and trapped by the lasers. This is the essence of the Gallagher–Pritchard model [4] of these collisions.

The first observations of trap-loss collisions were made for Na in a spontaneous-force optical trap [5, 6], but it was not possible to determine whether the collisions involved excited states or not. The first unambiguous observations of excited-state trap-loss collisions were made in Cs [7, 8], where a linear dependence of the trap-loss rate on the intensity of the trapping laser was observed. The observed rates were larger than predicted, however. Motivated by the Gallagher–Pritchard model prediction of the frequency dependence of the trap-loss rate, an additional "catalysis laser" was also applied to the trap. This submegahertz bandwidth laser could be tuned over a -1 GHz $< \Delta < 0$ frequency range, where Δ is the detuning of the laser from the atomic resonance, sufficient to test the predicted dependence. The trap-loss rate was observed to agree with the predicted Δ^{-2} dependence for large detunings. The experimental confirmation of the Δ^{-2} dependence, as well as a quantitative agreement between the model and the experiment at large detunings, suggested that the trap-loss collisions could be described by the model for large detunings.

The Gallagher–Pritchard model received additional support from the calculations of Julienne and Vigue [9], who added the effects of fine structure to the calculations and modified the model to have the correct high-temperature as well as low-temperature behavior. They achieved quantitative agreement with the small-detuning Cs measurement and, in addition, pointed out that long-lived dipole-forbidden molecular states could be important for Na, K, and Rb. Band and Julienne [10] performed an optical Bloch equation analysis of the large-detuning case for Cs and again obtained good agreement with the experiment.

The present paper is motivated by a recent series of experiments on Rb [1 - 3] that reveal serious disagreements with the models and suggest that the hyperfine structure introduces important features that have been

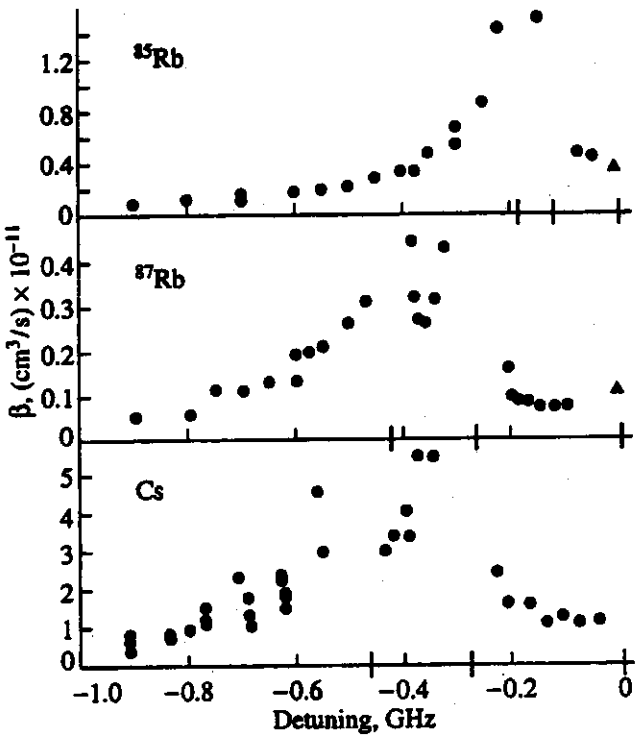

Fig. 1. Measurements of trap-loss collision rates for ^{85}Rb, ^{87}Rb, and Cs as a function of the detuning of the laser from the highest energy excited-state hyperfine level. The Cs data are from [8], the Rb data that are shown with circles are from [3], and the Rb data that are shown with rectangles are from [2]. Additional marks along the detuning axes show the positions of allowed atomic transitions from the upper hyperfine level of the ground state.

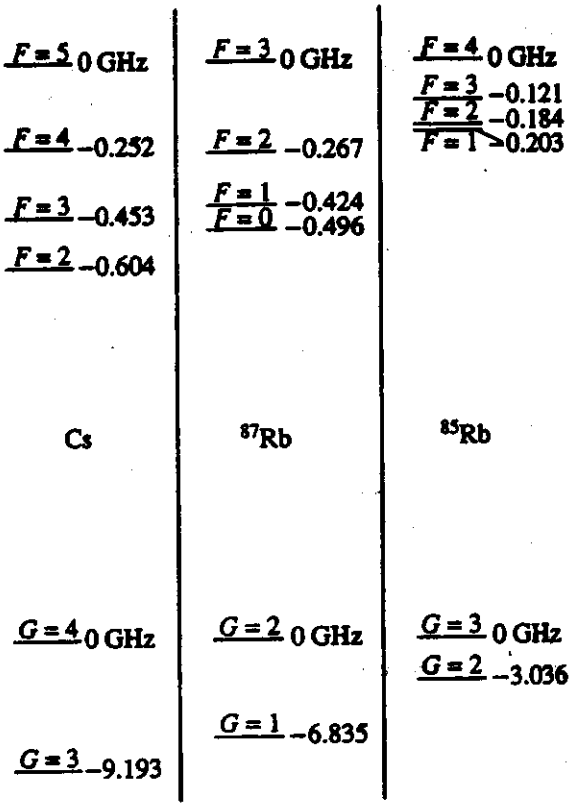

Fig. 2. The atomic hyperfine structures of the $S_{1/2}$ (lower part) and $P_{3/2}$ (upper part) states of ^{87}Rb, ^{85}Rb, and Cs. For purposes of comparison of the experimental results among the different atoms, we have adjusted the gross energy scales so that each of the highest energy hyperfine states are at zero energy.

left out of the models to date. The data are shown in Fig. 1. The detuning dependences of the trap-loss rates (or "trap-loss spectra") for the two isotopes of Rb, ^{85}Rb and ^{87}Rb are shown along with the corresponding spectra for Cs. First, it is clear that the Rb trap-loss rates are much smaller than those for Cs, in contrast to prediction [9]. Second, and more interesting, are the differing shapes of the spectra for the three species. The width of the trap-loss spectrum for each isotope seems to closely correlate with the amount of excited-state hyperfine splitting. For reference, in Fig. 2 we show the relevant atomic hyperfine structure, and in Fig. 1 we have included arrows at the positions of the allowed atomic hyperfine transitions for atoms that are in the $F = I + 1/2$ ground-state hyperfine level, as is the case for the traps used in these experiments. Another interesting feature of these spectra is the strong isotopic distinction between ^{87}Rb and ^{85}Rb at small detunings, whereas at large detunings the loss rates are equal, within errors. In addition, the ^{87}Rb spectrum shows evidence of peaks near the positions of the atomic excited-state hyperfine structure. The data strongly suggest that hyperfine effects, in particular excited-state hyperfine structure, are very important for determining the trap-loss collision dynamics and rates. Indeed, the small percentage difference in the mass of the Rb isotopes makes any alternative explanation very difficult to conceive.

Given the importance of hyperfine structure for trap-loss collisions, we have calculated the long-range potential curves, including hyperfine interactions, for the $P_{3/2}$ levels of alkali dimers, with the intent of identifying more precisely what the role of the hyperfine interaction is for the experiments that have been done to date, as well as making qualitative predictions for other possible experiments. In Section 2, we present the calculations of the long-range potential curves. In Section 3, we consider what features of the data of Fig. 1 can be understood in terms of these curves and simple estimates based on these curves. In Section 4, we identify new experiments that are suggested by these curves.

2. CALCULATIONS OF THE HYPERFINE STRUCTURE MANIFOLD

In this section, we present the calculations of the adiabatic potential curves for alkali dimers that correlate to one of the atoms being in the ground level and the other being in the first excited ($P_{3/2}$ or $P_{1/2}$) level, including both fine and hyperfine structure. The corresponding

potentials neglecting hyperfine structure were calculated by Movre and Pichler [11].

Before proceeding with the calculations, it is useful to consider the molecular hyperfine structure in the limit of large interatomic separations. This is obtained in a straightforward manner from the atomic hyperfine structure shown in Fig. 2 and is displayed in Fig. 3 for the case of ^{87}Rb. The hyperfine structure of the ground electronic states consists of three levels whose energies differ by the atomic ground-state hyperfine splitting. In all the trap-loss experiments done to date, the atoms begin in the uppermost of the three levels. If one atom is excited to the $P_{3/2}$ state, eight different hyperfine levels are possible, as shown. The eight levels are separated into two sets of four, depending on which ground-state hyperfine level the unexcited atom is in. The experiments done to date all involve excitation to the upper four levels (i.e., $2 + 2 \longrightarrow 2 + F$, for ^{87}Rb). The effect of the dipole–dipole interaction at finite internuclear separations will be to mix these various levels, as explained in the rest of this section. For the ground states, the dipole-dipole interaction has no first-order effect, and the resulting potentials are thus basically flat at the interatomic separations considered here.

The Hamiltonian to be diagonalized is

$$H = H_{A1}(\mathbf{r}_1) + H_{A2}(\mathbf{r}_2) + V_{DD}(\mathbf{r}_1, \mathbf{r}_2; \mathbf{R}). \qquad (1)$$

Here, $\mathbf{r}_1$ and $\mathbf{r}_2$ are the positions of the two electrons measured with respect to their associated nuclei; H_A is the Hamiltonian of a free atom, including fine and hyperfine structure; $V_{DD}(\mathbf{r}_1, \mathbf{r}_2; \mathbf{R}) = -e^2(2z_1z_2 - x_1x_2 - y_1y_2)/R^3$ is the electrostatic dipole–dipole interaction; and the subscripts 1 and 2 refer to the two atoms. The Hamiltonian is invariant on rotations about the interatomic axis and on interchange of the two atoms. Thus, the molecular states can be described by ϕ, the component of the total angular momentum (excluding rotation) along the axis, and on being even (g) or odd (u) upon interchange of the two atoms (electrons and nuclei).

We choose to perform the calculations in a basis of eigenstates of $H_{A1} + H_{A2}$. In this basis, only the matrix elements of V_{DD} have to be calculated, and the calculation is simplified by using angular momentum algebra. We define the notation $|a; b\rangle$ to denote a product state of atom 1 in atomic state a and atom 2 in atomic state b. Furthermore, the atomic states are denoted by the quantum numbers G and m_G for an atom in the $^2S_{1/2}$ state in hyperfine level G and Zeeman sublevel m_G and J, F, and m_F for an atom in a Zeeman sublevel of the ^2P_J state. Thus, a molecular state is given in terms of the atomic states as

$$|\phi_u^g GJFm_F\rangle = (|Gm_G; JFm_F\rangle \pm |JFm_F; Gm_G\rangle)/\sqrt{2}, \qquad (2)$$

with $m_G = \phi - m_F$. Note that there are a number of such states for a given ϕ: for example, the $6u$ molecular

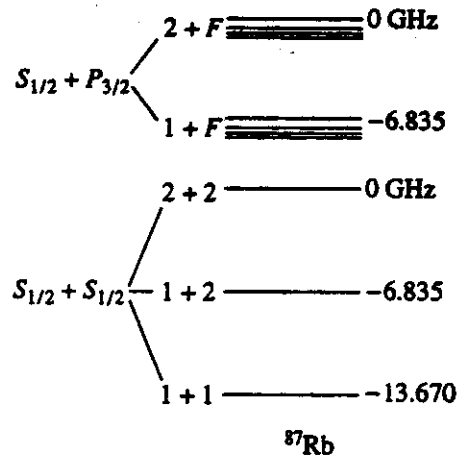

Fig. 3. The molecular hyperfine structure of the $S_{1/2} + S_{1/2}$ and $S_{1/2} + P_{3/2}$ states of ^{87}Rb at infinite interatomic separations. The experiments discussed in the text involve excitation from the 2 + 2 ground state to the 2 + F excited states of ^{87}Rb and the analogous states for the other atoms.

states of ^{85}Rb (I = 3/2) are linear combinations of $|6u3\frac{3}{2}44\rangle$, $|6u3\frac{3}{2}43\rangle$, $|6u3\frac{3}{2}33\rangle$, and $|6u2\frac{3}{2}44\rangle$.

This basis, in which all the angular momenta are coupled, is more convenient for this problem than an uncoupled basis for several reasons. The most important reason is the conceptual advantage that, since in most optical traps the atoms are all in a well-defined ground-state hyperfine level (usually $G = I + 1/2$), the molecular states naturally correlate to the atomic states at infinite interatomic separations. The second reason is that the spin orbit and hyperfine interactions (both magnetic dipole and electric quadrupole) are diagonal in this basis; only the dipole–dipole interaction has off-diagonal matrix elements. The spin–orbit and hyperfine interactions only enter the problem through the unperturbed energies of the various states. Finally, the increased complexity of the dipole–dipole matrix elements in the coupled basis is considerably simplified by standard angular momentum algebra.

We now give the matrix elements for the dipole–dipole interaction. They are

$$\begin{aligned}
&\langle \phi_u^g G'J'Fm_F'|V_{DD}|\phi_u^g GJFm_F\rangle \\
&\quad = \pm\langle G'\phi - m_F'J'Fm_F'|V_{DD}|JFm_FG\phi - m_F\rangle \\
&\quad = \pm\left(\frac{-e^2}{R^3}\right)\Big(2\langle G'\phi - m_F'|r_0|JFm_F\rangle\langle J'Fm_F'|r_0|G\phi - m_F\rangle \\
&\qquad + \langle G'\phi - m_F'|r_{+1}|JFm_F\rangle\langle J'Fm_F'|r_{-1}|G\phi - m_F\rangle \\
&\qquad + \langle G'\phi - m_F'|r_{-1}|JFm_F\rangle\langle J'Fm_F'|r_{+1}|G\phi - m_F\rangle\Big).
\end{aligned} \qquad (3)$$

We will be considering the potentials only at distances where the spin–orbit interaction is much larger than the dipole–dipole interaction, so we will now specialize to $J' = J$. The Wigner–Eckhart theorem is used to express the matrix elements of the spherical vectors $r_{0,\pm1}$ in terms of the reduced matrix elements $\langle J\|r\|1/2\rangle$. Defining

$$C_3 = \frac{e^2\langle 3/2\|r\|1/2\rangle^2}{2R^3}, \tag{4}$$

the final result for the matrix elements of V_{DD} is

$$\begin{aligned}
&\langle \phi_u^s G J F m_F' | V_{DD} | \phi_u^s G J F m_F \rangle \\
&= \pm\frac{C_3}{R^3}(-1)^{2I+G+G'+F+F'+m_F+m_F'}\left(J+\frac{1}{2}\right) \\
&\times\sqrt{(2G+1)(2G'+1)(2F+1)(2F'+1)} \\
&\times\begin{Bmatrix} F & 1 & G \\ 1/2 & I & J \end{Bmatrix}\begin{Bmatrix} F & 1 & G' \\ 1/2 & I & J \end{Bmatrix} \\
&\times\left[2\begin{pmatrix} F & G & 1 \\ -m_F' & \phi-m_F & 0 \end{pmatrix}\begin{pmatrix} F & G' & 1 \\ -m_F & \phi-m_F' & 0 \end{pmatrix}\right. \\
&-\begin{pmatrix} F & G & 1 \\ -m_F' & \phi-m_F & 1 \end{pmatrix}\begin{pmatrix} F & G' & 1 \\ -m_F & \phi-m_F' & 1 \end{pmatrix} \\
&\left.-\begin{pmatrix} F & G & 1 \\ -m_F' & \phi-m_F & -1 \end{pmatrix}\begin{pmatrix} F & G' & 1 \\ -m_F & \phi-m_F' & -1 \end{pmatrix}\right].
\end{aligned} \tag{5}$$

The adiabatic potentials are the eigenvalues found by standard numerical diagonalization of the Hamiltonian matrix for various values of R.

Examples of the adiabatic potentials are shown in Figs. 4 - 7. For convenience, the potentials are plotted as a function of $C_3/\hbar R^3$. Note that there are two distance scales where avoided crossings occur for the $P_{3/2}$ potentials. These distance scales correspond to the distances where the dipole–dipole interaction is comparable to the excited-state hyperfine splittings at large separations and where the dipole–dipole interaction is comparable to the ground-state splittings at smaller separations.

3. DYNAMICAL EFFECTS OF THE HYPERFINE STRUCTURE

In this section, we will consider some consequences of the adiabatic potentials for trap-loss collisions. We will present a straightforward extension of the Gallagher–Pritchard model to include hyperfine structure. This will provide a framework for our discussion of how the hyperfine structure can be expected to modify the dynamics of trap-loss collisions.

We first review the simple Gallagher–Pritchard model [4]. Atoms are assumed to be uniformly distributed in space, i.e., the number of atoms at distance R from a given atom is $n4\pi R^2 dR$, where n is the number density of atoms. These atoms are excited by the laser at the rate $\sigma(R)I/\hbar\omega$. Once excited, the atoms are accelerated toward each other by the attractive potentials. If the acceleration is strong enough, the atoms can reach small interatomic separations where energy transfer can occur. The probability of reaching this energy transfer region is $\exp[-t(R)/\tau]$, where $t(R)$ is the time required to reach the energy transfer region and $1/\tau$ is the spontaneous emission rate. The total trap-loss rate is found by integrating over all R, multiplied by the probability of energy transfer $P_{\Delta E}$:

$$\beta = P_{\Delta E}\int 4\pi R^2 dR\frac{\sigma(R)I}{\hbar\omega}e^{-t(R)/\tau}. \tag{6}$$

We will ignore the initial velocities of the atoms. Julienne and Vigue [9] have shown that this is a poor assumption for small laser detunings (i.e., detunings comparable to the natural linewidth), but we will mostly be interested in large detunings where the acceleration by the excited-state potential is sufficiently strong that the initial velocities should not matter much.

Note that the trap-loss rate given by equation (6) naturally separates into two factors. The first, $P_{\Delta E}$, gives the probability of energy transfer and should be relatively insensitive to the dynamics of the collision at large R. The rest of equation (6) describes the dynamics of the collision. Thus, the dynamics include the excitation by the laser and the motion of the atom pairs on the excited-state potential curve, which is also strongly affected by spontaneous emission.

We note that, as long as the laser is not too close to the allowed atomic resonance transitions, $\sigma(R)$ should be strongly peaked at interatomic separations obeying the resonance condition $\hbar\Delta = -C_3/R_0^3$. Then, the slowly varying factors R^2 and $t(R)$ can be removed from the integral, so

$$\beta = \frac{4\pi^2 C_3}{3\hbar}r_e f c\frac{I}{\hbar\omega}P_{\Delta E}\frac{e^{-t(R_0)/\tau}}{\Delta^2}, \tag{7}$$

where r_e is the classical electron radius, c is the speed of light, and f the oscillator strength. For the case of motion on a pure R^{-3} potential, $t(R_0) \approx 0.746\sqrt{\mu R_0^5/2C_3} = 0.746\sqrt{\mu/2}C_3^{1/3}/(\hbar\Delta)^{5/6}$. Defining $\Delta_\tau = (0.746\sqrt{\mu/2}C_3^{1/3}/\hbar^{5/6}\tau)^{5/6}$, we get

$$\beta = \frac{4\pi^2 C_3}{3\hbar}r_e f c\frac{I}{\hbar\omega}P_{\Delta E}\frac{\exp[-(\Delta_\tau/\Delta)^{5/6}]}{\Delta^2}. \tag{8}$$

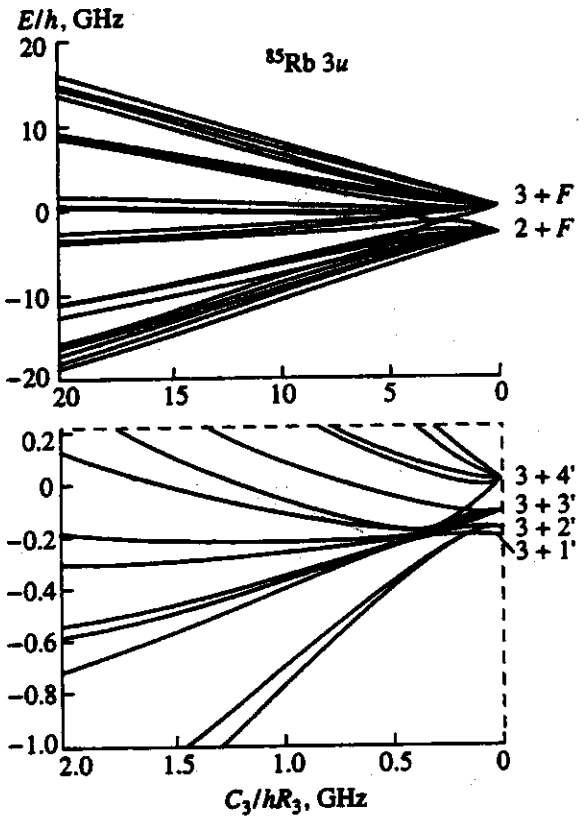

Fig. 4. The $3u$ potential curves of ^{85}Rb, including an expanded view of these curves in the region of excited-state hyperfine recoupling (bottom). In this and the following figures, numerical values of F are denoted with a prime, while numerical values of G are given without the prime.

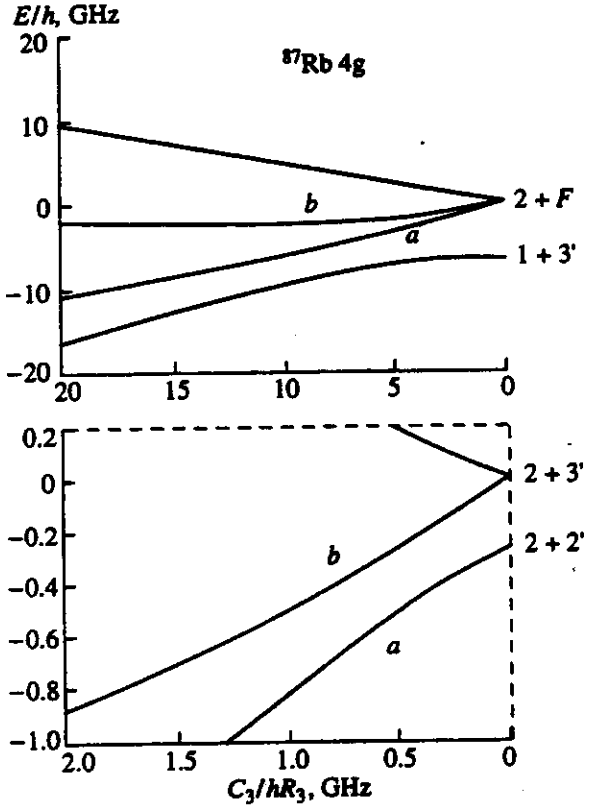

Fig. 5. Curves analogous to Fig. 4 for the $4g$ states of ^{87}Rb. If the motion is purely adiabatic, curve a will contribute to trap loss but b will not since it becomes repulsive at small distances.

This predicts a maximum in the detuning dependence at $\Delta \approx -0.35\Delta_t$. For Cs, with $C_3 = 79$ eV Å^3, and Rb, with $C_3 = 71$ eV Å^3, the maximum should be around -40 MHz. From Fig. 1, we see that this is not even close for Cs and ^{87}Rb.

To try to improve on this by accounting for the hyperfine structure, it is necessary to provide for the excitation to the various potential curves as well as the subsequent motion on those curves. Thus, we write

$$\beta = P_{\Delta E}\int 4\pi R^2 dR \sum_i \frac{\sigma_i(R) I}{\hbar\omega} \sum_j S_{ij}(R). \qquad (9)$$

Besides generalizing the absorption rate to potential curve i via $\sigma_i(R)$, with the factor $S_{ij}(R)$ we have allowed for the possibility that, due to the motion of the atoms, nonadiabatic transitions may occur to other potential curves j. $S_{ij}(R)$ must account for spontaneous emission as well. For simplicity, we have ignored a possible dependence of $P_{\Delta E}$ on j. This is probably a reasonable assumption if the dominant trap-loss mechanism is radiative redistribution, which can happen for any attractive potential. Fine-structure changing collisions may have a dependence on j because only a small number of states can cause trap loss through this mechanism [9].

We can now make some qualitative statements about how the hyperfine interactions affect the trap-loss rates, according to this extension of the Gallagher–Pritchard model. First, if a particular potential curve $V_i(R)$ is optically allowed for absorption from the occupied ground states of Fig. 3 (2 + 2 for ^{87}Rb) and if it is fully attractive to small interatomic separations, then the factor S_{ij} will be just the exponential factor in equation (6), so the contribution to the trap-loss rate from this curve will have a detuning dependence of the form of equation (8). An example of this would be curve a in Fig. 5. Curve b is also attractive at large distance but becomes repulsive at small distance, so would not contribute to trap loss in the absence of nonadiabatic motion. Second, consider a curve such as curve c in Fig. 6. At large separations, it is repulsive but has an avoided crossing with an attractive curve coming from above and becomes attractive. For this curve, the trap-loss spectrum will have roughly the shape of equation (6), but shifted in frequency by an amount ≈ -0.17 GHz (obtained by extrapolation to infinite separation), and (crudely) truncated for $\Delta < -0.23$ GHz. Note that there is significant contribution to the blue of the corresponding atomic hyperfine resonance. Third, curve d in Fig. 7 is attractive at large distance but becomes repulsive due to the

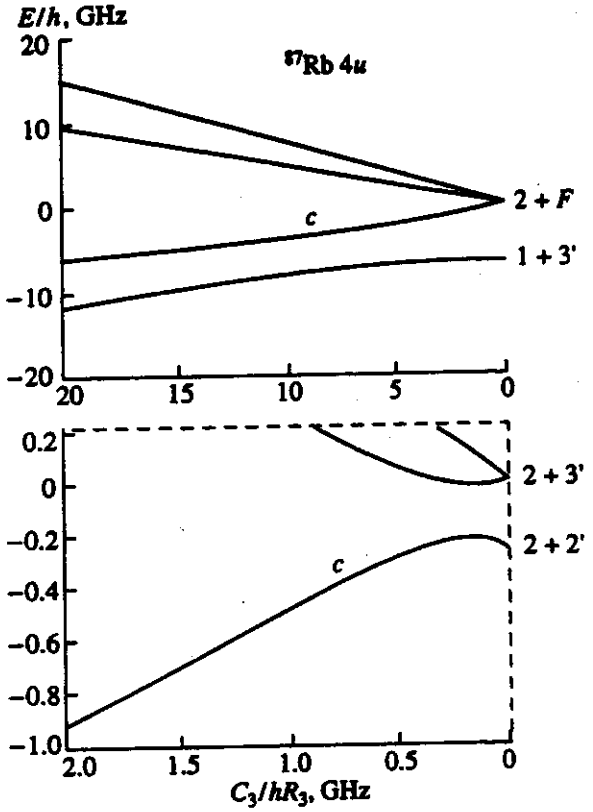

Fig. 6. Curves analogous to Fig. 4 for the $4u$ states of ^{87}Rb. Excitation to curve c will give trap loss at a detuning to the red of the 2 + 2' atomic hyperfine state.

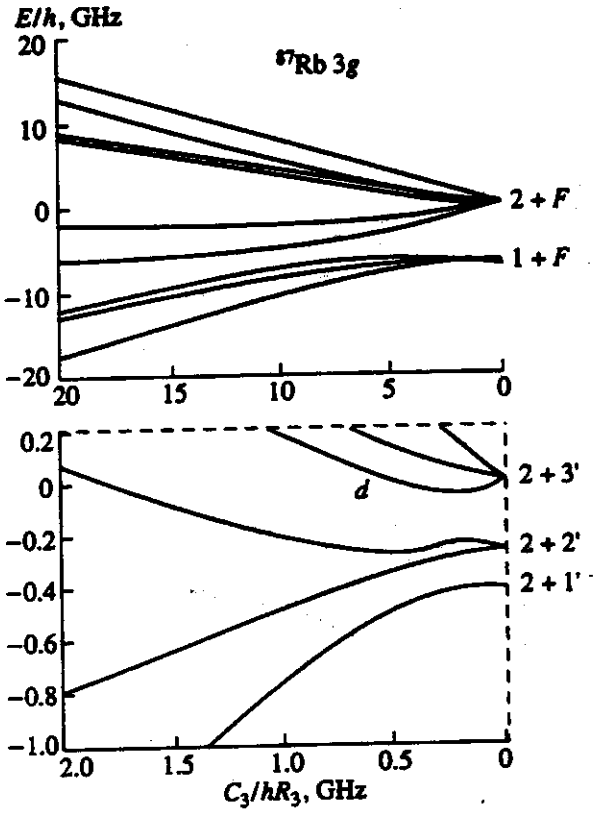

Fig. 7. Curves analogous to Fig. 4 for the $3g$ states of ^{87}Rb. Curve d will not contribute to trap loss in the absence of nonadiabatic motion along the potentials.

avoided crossing. This curve can contribute to trap loss only if there is a significant nonadiabaticity due to the nonzero velocity of the atoms upon reaching the region of the avoided crossing. If so, acceleration can continue along the attractive potential.

With these ideas in mind, we now consider what features of the trap-loss spectra shown in Fig. 1 can be explained. If we neglect nonadiabatic effects on the dynamics, the only potential curves that can contribute to trap loss are those that are attractive at small R. There are no such optically allowed potentials that correlate to the uppermost hyperfine state (i.e., 2 + 3' for ^{87}Rb) at $R = \infty$. This is consistent with the low trap-loss rates observed for ^{87}Rb, ^{85}Rb, and Cs at small detunings but does not explain why there is any trap loss at all.

As more negative detunings are considered, more attractive potentials are available to be excited, and therefore the trap-loss rate increases. Note that this occurs to the red of the next lower hyperfine resonance (i.e., 2 + 2' for ^{87}Rb) due to the maxima of curves such as shown in Fig. 6 being higher in energy than the corresponding atomic state. The bulk of the attractive potentials originate from the lowest hyperfine states, so it is not surprising that the trap-loss rates are observed to peak near the positions of these states in all three systems.

We now estimate, using standard two-state theory, the adiabaticity of the motion along the potential curves. Possible nonadiabatic effects can arise from rotational coupling, external fields, or radial coupling. We will find that radial coupling is likely to be the most important effect for these collisions. While the assumptions of the theory, namely, only two coupled states, constant potential coupling, no acceleration, and linear potentials, are not precisely met for ultracold collisions, estimates based on the Landau–Zener theory should give a good indication of when mostly adiabatic or diabatic behavior is to be expected.

Nonadiabatic transitions caused by rotational coupling have been considered by Russek [12]. The rotation of the colliding atoms can cause transitions of $\Delta\Omega = \pm 1$ at crossings of curves of different Ω. Russek finds the transition probability in the Landau–Zener approximation to be $1 - e^{-2\pi\gamma}$, where

$$\gamma = \frac{\omega^2 |L|^2}{\hbar v_R \left| (d/dR)(\varepsilon_2 - \varepsilon_1) \right|_{R = R_x}}. \qquad (10)$$

Here, ω is the rotational frequency, L is a matrix element of angular momentum raising and lowering operators, v_R is the radial velocity, and $\left| (d/dR)(\varepsilon_2 - \varepsilon_1) \right|_{R = R_x}$ is the difference of the forces experienced on the two curves. In order of magnitude, $\omega \sim v/R$, $L \sim \hbar$, $v_R \sim v$, and $\varepsilon_2 - \varepsilon_1 \sim C_3/R^3$, where v is a typical thermal velocity. Thus, we estimate $\gamma \sim v/6\pi R(V/h) \sim 0.007$ using

$v = 20$ cm/s, $R \sim 300$ Å, and $V/h \sim 50$ MHz. Note that we have overestimated by choosing $v_R \sim v$ since the atoms are accelerated toward each other before reaching a crossing. Thus, rotational coupling should not be important, except in cases where the slope difference $|(d/dR)(\varepsilon_2 - \varepsilon_1)|_{R=R_x}$ becomes small.

Nonadiabatic coupling could also result from the external magnetic field of as high as a few Gauss that exists in a typical optical trap. For this, we estimate $(\mu_B B)^2/(\hbar v_R)|(d/dR)(\varepsilon_2 - \varepsilon_1)|_{R=R_x} \sim 0.03$ or less for $v_R > v$. Again, the magnetic coupling of the curves should be negligible.

For radial coupling, which can produce nonadiabatic transitions between states of the same symmetry, the standard Landau–Zener formula [13] for the transition probability is

$$p = \exp\left(-\frac{2\pi V_{12}^2}{\hbar v|(d/dR)(\varepsilon_2 - \varepsilon_1)|_{R=R_x}}\right). \quad (11)$$

The radial coupling V_{12} is determined as one-half the closest distance between the adiabatic potential curves, and ε_2 and ε_1 are the diabatic potentials. It is evident from the figures that a wide variety of avoided crossings exists for various potential curves, and the motion can range from being strongly diabatic to being strongly adiabatic. For example, in Fig. 4, a number of curves that originate from the 3 + 4', 3 + 3', and 3 + 2' states coalesce at a detuning of −0.2 GHz and a distance corresponding to $C_3/hR^3 = 0.35$ GHz. Atoms excited at −0.05 GHz, for example, would be moving rapidly enough that the motion would be diabatic, if the two-level formula gives a reasonable estimate. Obviously, a proper treatment would need to include at least all of the six interacting potentials to understand the dynamics.

Curve *d* in Fig. 7 is an example of the opposite extreme. Here, the crossing is strongly avoided, and the transition probability according to equation (11) is very small. According to this model, trap loss would be unlikely to arise from excitation to this curve.

We have explicitly assumed that the absorption occurs when the laser and the potential curves are resonant, i.e., the classical Franck–Condon principle is obeyed. In some cases, this may be a poor assumption. In particular, it is known that, in the region of an avoided crossing, the absorption spectrum is substantially modified [14]. This problem is worthy of further study.

To summarize, it is probable that radial coupling dominates the nonadiabatic dynamics and will have to be considered in detail in order to quantitatively understand the trap-loss spectra in certain regions, especially for small detunings.

4. PREDICTED EFFECTS

The potentials suggest a variety of new effects as well as providing some qualitative understanding of the shapes of the trap-loss spectra. First, we note that, in the absence of nonadiabatic effects, trap loss is possible only for the attractive potentials that arise from the lowest energy excited hyperfine levels. This may well account for the observed peaking of the experimental trap-loss spectra near the lowest hyperfine levels in all three systems studied to date, see Fig. 1. Thus, we also expect that the trap-loss rate coefficients in general will be larger for traps in which many atoms are in the lowest ground-state hyperfine state. An example of such a trap is the dark spot trap of Ketterle *et al.* [15]. In particular, the spectra arising from detunings just red of the lowest ground-state hyperfine state should be virtually free of nonadiabatic effects. We suggest that this may the best type of experiment for making quantitative comparisons of the experiment to fairly simple models of the collision dynamics.

A second effect that should be observable is trap loss arising for frequencies in regions for which absorption is dipole forbidden at large distances. For example, referring to Fig. 3, absorption from the 2 + 2 state to the 1 + *F* manifold of states is dipole forbidden at large interatomic separations. However, at interatomic separations where the dipole–dipole interaction is comparable to the ground-state hyperfine splitting, the 1 + *F* states are mixed with the 2 + *F* states, so absorption will be allowed. On an absolute scale, the rates will be reduced due to the small number of atom pairs available to be excited at these short distances. However, at these distances, the survival probability to small *R* will be large, and so multiple traversals of the energy transfer region will enhance the trap-loss rates. Effects similar to these have been observed for associative ionization of sodium [17, 18].

Third, we note the existence of weakly bound long-range molecular states that arise from hyperfine coupling. These are analogous to the well-known long-range states, referred to as pure long-range molecular states, that arise from fine-structure decoupling [16]. Two classes of such states exist, corresponding to decoupling of either the excited-state or ground-state hyperfine interactions. Examples are shown in Figs. 4 and 5. Resolving the bound levels of these states will be difficult but may be possible for those minima arising from the larger ground-state hyperfine separations.

5. CONCLUSION

We have presented the long-range interatomic potentials for alkali dimers at distances where the hyperfine interaction is important. The excited-state hyperfine interaction causes structure in the curves on the frequency variation observed in experiments on Cs and Rb [1, 3, 7, 8], while the ground-state hyperfine interaction should lead to structure in spectral regions not yet probed in these experiments, especially when ground-state atoms in the lower hyperfine state are involved. We have argued that the presence of avoided crossings of these potentials in the region that has been probed by recent experiments suggests that nonadiabatic dynamics are important for understanding these

experiments. Other new collisional effects that arise from hyperfine interactions have been identified as well. It is clear that any realistic model of ultracold collisions must include hyperfine interactions.

The importance of hyperfine interactions for understanding excited-state ultracold collisions demonstrates the unique sensitivity of these collisions to extremely weak interactions. In a sense, this is unfortunate since the increased complexity that arises tends to obscure the role played by the fundamentally more interesting spontaneous emission of light during the collisions. It may be possible to reduce this increased complexity by careful design of experiments to probe regions of the potentials where both distortions of the curves due to avoided crossings and nonadiabatic effects are not important.

ACKNOWLEDGMENTS

This research is supported by the National Science Foundation, the Office of Naval Research, the Air Force Office of Scientific Research, and the Packard Foundation. T.W. is an Alfred P. Sloan Research Fellow.

REFERENCES

1. Hoffmann, D., Feng, P., Williamson, R., *et al.*, 1992, *Phys. Rev. Lett.*, **69**, 753.
2. Wallace, C., Dinneen, T., Tan, K., *et al.*, 1992, *Phys. Rev. Lett.*, **69**, 897.
3. Feng, P., Hoffmann, D., and Walker, T., 1993, *Phys. Rev. A*, **47**, R3495.
4. Gallagher, A. and Pritchard, D., 1989, *Phys. Rev. Lett.*, **63**, 957.
5. Raab, E., Prentiss, M., Cable, A., *et al.*, 1987, *Phys. Rev. Lett.*, **59**, 2631.
6. Prentiss, M., Cable, A., Bjorkholm, J., *et al.*, 1988, *Opt. Lett.*, **13**, 452.
7. Sesko, D., Walker, T., Monroe, C., *et al.*, 1989, *Phys. Rev. Lett.*, **63**, 961.
8. Walker, T., Sesko, D., Monroe, C., *et al.*, 1989, *The Physics of Electronic and Atomic Collisions, XVI Int. Conf.*, Dalgarno, A., Freund, R., Koch, P., *et al.*, Eds. (AIP).
9. Julienne, P. and Vigue, J., 1991, *Phys. Rev. A*, **44**, 4464.
10. Band, Y. and Julienne, P., 1992, *Phys. Rev. A*, **46**, 330.
11. Movre, M. and Pichler, G., 1977, *J. Phys. B*, **10**, 263.
12. Russek, A., 1971, *Phys. Rev. A*, **4**, 1918.
13. Zener, C., 1932, *Proc. R. Soc. London, A*, **137**, 696.
14. O'Callaghan, M., Gallagher, A., and Holstein, T., 1985, *Phys. Rev. A*, **32**, 2754.
15. Ketterle, W., Davis, K., Jaffe, M., *et al.*, 1993, *Phys. Rev. Lett.*, **70**, 2253.
16. Stwalley, W., Uang, Y.-H., and Pichler, G., 1978, *Phys. Rev. Lett.*, **41**, 1164.
17. Wagshul, M. *et al.*, 1993, *Phys. Rev. Lett.*, **70**, 2074.
18. Bagnato, V. *et al.*, 1993, *Phys. Rev. Lett.*, **70**, 3225.